ELSEVIER

1 June 1998

Optics Communications 151 (1998) 366–373

OPTICS COMMUNICATIONS

Full length article

# Spectroscopic characterization of $BaLiF_3:Co^{2+}$ crystals

Marcos Duarte [1], Evely Martins [2], Sonia L. Baldochi, Spero P. Morato, Nilson D. Vieira Jr., Martha M.F. Vieira *

*Instituto de Pesquisas Energéticas e Nucleares, P.O. Box 11049, CEP 05422-970 São Paulo, SP, Brazil*

Received 14 July 1997; revised 24 November 1997; accepted 9 December 1997

**Abstract**

$BaLiF_3$ crystals doped with two different concentrations of the transition metal ion $Co^{2+}$ (0.05 and 0.44 mol%) were studied. The observed optical properties of both crystals are correctly described by the model of point charges of the $Co^{2+}$ ion in a pure octahedral symmetry. Two intense absorption bands were noticed: one peaking at 20000 $cm^{-1}$ (500 nm), corresponding to the $^4T_1$ ($^4F$) → $^4T_1$ ($^4P$) transition and the other peaking at 8264 $cm^{-1}$ (1210 nm), corresponding to the $^4T_1$ ($^4F$) → $^4T_2$ ($^4F$) transition, with normalized bandwidths of approximately 20%. A weaker band at 16667 $cm^{-1}$ (600 nm) was also observed, corresponding to the $^4T_1$ ($^4F$) → $^4A_2$ ($^4F$) transition. $BaLiF_3:Co^{2+}$ crystals present a single emission broad band peaking at 6670 $cm^{-1}$ (1500 nm), corresponding to the $^4T_2$ ($^4F$) → $^4T_1$ ($^4F$) transition, with full width at half maximum of 280 nm at 12 K, being a promising candidate to a laser medium suitable for telecommunication devices.


*PACS:* 78.50.W
*Keywords:* Laser materials; Optical spectroscopy; Luminescence; $Co^{2+}$-doped

## 1. Introduction

The requirement for lasers with specific characteristics (high output powers, particular spectral region of operation, temporal pulse width, tuning range, etc.), has encouraged the discovery and the improvement of many laser active media. Among the lasers under development, the class of vibronic lasers stands out, as the $Ti:Al_2O_3$ [1] and other systems [2]. In this laser category the active species is a substitutional ion in a host crystal, which usually creates a strong interaction with the crystalline lattice (note that not all transition metal ions states interact strongly with the lattice, e.g. R lines of ruby. See for example Ref. [3]). Due to this interaction the optical transitions present broad bands, allowing easy pumping by other lasers or lamps, and laser tuning and optical amplification in a wide wavelength range [2].

Much effort has been concentrated on developing lasers for the near infrared region, which is of interest for medical applications and for signal transmission in optical fibers. In spite of this, few laser sources are available in this region. The main active laser media operating in the 1500 nm range are: $Co^{2+}:MgF_2$ from 1460 to 2110 nm [4], $Tl^0(1):KCl$ from 1400 to 1700 nm [5], $Ni^{2+}$:CAMGAR from 1380 to 1590 nm [6], and $Cr^{4+}$:YAG from 1340 to 1560 nm [7]. Additionally, ionic hosts doped with transition metal ions, like $Co^{2+}$ or $Ni^{2+}$, usually show emission bands in the near infrared region and some of these transitions are particularly laser active.

* Corresponding author. E-mail: mmvieira@net.ipen.br
[1] Permanent address: Escola de Educação Física, Universidade de São Paulo, Av. Mello Moraes, 65, CEP 05508-900 São Paulo, SP, Brazil.
[2] Present address: Instituto de Estudos Avançados, IEAv/CTA, Rodovia dos Tamoios km 5,5, CEP 12231-970 Sao José dos Campos, SP, Brazil.

0030-4018/98/$19.00 
*PII* S0030-4018(97)00741-4

Recently, several studies on the ionic crystal $BaLiF_3$, either in its pure form [8] or doped with Pb [9,10] and $Ni^{2+}$ [11,12] have been reported. The $Ni^{2+}$ doped $BaLiF_3$, for example, presents an emission band centered at 1500 nm with 250 nm full width at half maximum (FWHM), at room temperature. This crystal has been very promising as a vibronic active laser medium, but to our knowledge laser action has not yet been reported.

The cobalt (Co) ion has been successfully used as a laser active ion in crystals presenting perovskite structure [13]. This work presents the spectroscopic characterization of $Co^{2+}$ doped $BaLiF_3$ crystals, with emphasis towards the laser capabilities in the near infrared region (1500 nm).

## 2. The crystal

The $BaLiF_3$ crystal presents a perovskite structure, specifically belonging to the fluoroperovskite family, $AMF_3$, where A and M stand for mono and divalent ions, respectively. Compared to the classic perovskite, the barium ($Ba^{2+}$) and lithium ($Li^+$) ions are in exchanged site positions as shown in Fig. 1, so this crystal is called an inverted fluoroperovskite [14]. The family $AMF_3$ allows the replacement of the A and M ions by several chemical elements without altering the basic properties. Crystals with fluoroperovskite structure have been extensively studied [15–17] and some of these crystals, such as $KZnF_3$ and $KMgF_3$, have presented laser action when doped with transition metal ions [18–20].

Fig. 1 shows the cubic structure unit cell (spatial group $O_h$-Pm3m) of the $BaLiF_3$ crystal. The $Li^+$ ion is in the center of an octahedron constituted of six fluoride ions and the $Ba^{2+}$ ion is in the center of a dodecahedron composed of 12 fluoride ions. The coordination numbers of the two ions are 6 and 12, respectively.

The cobalt doped $BaLiF_3$ crystals were grown at our laboratories by the Czochralski technique [21]. The starting materials for crystal growth were synthesized from $BaF_2$ and LiF, and purified by the zone refine technique in a HF reactive atmosphere. The growth was performed in a furnace where the synthesized material is mixed with $CoF_2$ in powder form. Alternatively, the impurity may be added during the synthesis. The mixture is melted under an inert argon atmosphere. Starting with a crystalline seed, the $BaLiF_3$:$Co^{2+}$ crystal is pulled from the melt. Typically, $BaLiF_3$:$Co^{2+}$ crystals presented a pink coloration and cylindrical dimensions of 5 cm length by 2 cm diameter from which samples for spectroscopic studies were prepared.

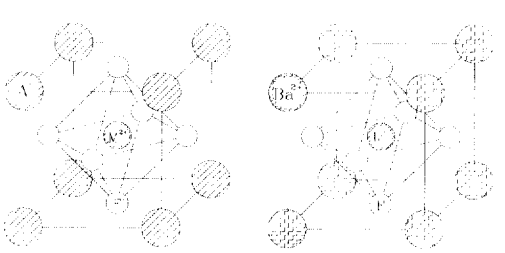

Fig. 1. Crystalline structure of the classic fluoroperovskite (left side) and the $BaLiF_3$ crystal (right side).

The position of the dopant $Co^{2+}$ ions is still a matter of debate. The crystallographic data suggests that the $Co^{2+}$ ion could replace two different sites in the $BaLiF_3$ host, the $Li^+$ site or the $Ba^{2+}$ site, although some indirect evidence from optical studies suggests that $Co^{2+}$ ions occupy a local octahedral environment. The $Li^+$ site presents pure octahedral symmetry, whereas the $Ba^{2+}$ site presents dodecahedral symmetry, which in first approximation is a cubic symmetry. We suppose that the similarity of their ionic radii favors a $Co^{2+}$ ion (0.69 Å radius) to replace a $Li^+$ ion (0.68 Å), particularly since the ionic radius of $Ba^{2+}$ is very different (1.34 Å). Another fact that supports this supposition is the analogy with the $BaLiF_3$:$Ni^{2+}$ crystal, where the dopant $Ni^{2+}$ ion predominantly (at least 85%) is on $Li^+$ site, measured by EXAFS (extended X-ray absorption fine structure) [22]. However, charge compensation is required and the mechanism involved is still unclear. Charge compensation provided by impurities is discarded. For example, an $O^{2-}$ impurity cannot affect the site symmetry at all, since the contamination by $O^{2-}$ in the crystal is much less than the $Co^{2+}$ ion concentration [14].

Two crystals with different Co concentrations were studied in this work. A concentration of 0.05 mol% was achieved by adding 3 mol% in the melt during the growth process, and the concentration of 0.44 mol% required 5 mol% in the melt. The Co concentration in the $BaLiF_3$ host was determined by neutron activation analysis [21].

## 3. Results and discussion

### 3.1. Optical absorption

The optical absorption properties of transition metal ions in ionic crystals have been studied for several decades and are characterized by broad absorption bands with FWHM of hundreds of nanometers. The broad absorption and emission spectra were due to the strong coupling of some electronic energy levels of the transition metal ion with the lattice phonons [23].

Optical absorption spectroscopy was performed in a commercial spectrophotometer (Cary 17D, Varian). For the low temperature measurements the samples were placed in a closed-cycle helium cryostat (Displex CS-202, Air Products) where the temperature could be varied from 10 to 300 K.

For the Co ion ($3d^7$) (see Fig. 2) the $BaLiF_3$ octahedral symmetry splits the ground state $^4F$ ($L = 3$, $S = 3/2$) in

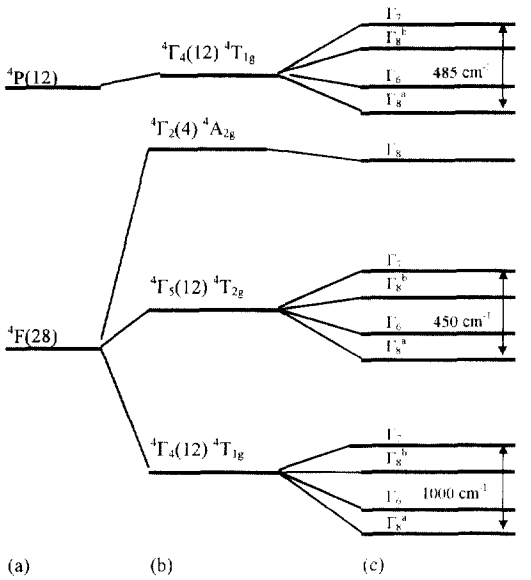


Fig. 2. $Co^{2+}$ ion in octahedral symmetry. (a) Free ion's spectral term; (b) ion in an intermediate field (LS coupling not included); (c) ion in an intermediate field (LS coupling included) with typical separation energy [24,25].

$^4T_2$ ($^4A_2$), $^4T_4$ ($^4T_1$) and $^4T_5$ ($^4T_2$), with a total degeneracy equal to 28 ($4 \times 1$, $4 \times 3$ and $4 \times 3$). The effect of the spin–orbit coupling is to split these levels further in $\Gamma_2$ ($^4A_2$) $\rightarrow \Gamma_8$, $\Gamma_4$ ($^4T_1$) $\rightarrow \Gamma_6 + \Gamma_7 + 2\Gamma_8$ and $\Gamma_5$ ($^4T_2$) $\rightarrow \Gamma_6 + \Gamma_7 + 2\Gamma_8$. The free ion first excited state $d^7$ is the $^4P$ ($L = 1$, $S = 3/2$); in the presence of an octahedral field it is reduced to $\Gamma_4$ ($^4T_1$). The introduction of the spin–orbit coupling consequently induces a new splitting $\Gamma_4$ ($^4T_1$) $\rightarrow$ $\Gamma_6 + \Gamma_7 + 2\Gamma_8$, with a total degeneracy equal to 12.

Fig. 3 shows the absorption spectra of a $BaLiF_3:Co^{2+}$ sample (0.44 mol% Co concentration) at 10 and 300 K. The $BaLiF_3:Co^{2+}$ optical absorption spectra are typical of $Co^{2+}$ ions in octahedral symmetry and are similar to the reported spectra for $KMgF_3:Co^{2+}$ [15], $MgO:Co^{2+}$ [24]. The $BaLiF_3:Co^{2+}$ strongest absorption bands peak at 20 000 cm$^{-1}$ (500 nm) and 8264 cm$^{-1}$ (1210 nm), correspond to the $^4T_1$ ($^4F$) $\rightarrow$ $^4T_1$ ($^4P$) and $^4T_1$ ($^4F$) $\rightarrow$ $^4T_2$ ($^4F$) transitions, respectively. Besides these two bands there is a weaker band at 16 667 cm$^{-1}$ (600 nm), which corresponds to the $^4T_1$ ($^4F$) $\rightarrow$ $^4A_2$ ($^4F$) transition. Table 1 lists the transitions and the respective absorption cross-sections. At low temperature there is no significant change in the absorption intensities. However, the absorption bands were shifted towards lower energies and their FWHM were narrower than at room temperature. For temperatures lower than 77 K two sets of sharp lines can be also seen in the infrared absorption band ($^4T_1$ ($^4F$) $\rightarrow$ $^4T_2$ ($^4F$) transition), which will be discussed in greater detail.

From the initial assignment of the absorption bands to the transitions, the crystal field parameter, $Dq$, and the Racah parameters, $B$ and $C$, may be calculated by diagonalization of the energy matrices following the Tanabe–Sugano model [26]. In this work, only the quartet terms are calculated for the $Co^{2+}$ ion, because they are responsible for the optical transitions observed. The computation of the quartet terms is straightforward, whereas the doublet terms require complex numerical calculations due to the high mixture of electronic configuration.

The crystal field parameter $Dq$ in $BaLiF_3:Co^{2+}$ is 936 cm$^{-1}$, and the Racah parameters $B$ and $C$ are 875 cm$^{-1}$ and 3850 cm$^{-1}$, respectively. The Tanabe–Sugano diagram for the $BaLiF_3:Co^{2+}$ based on the calculated values is shown in Fig. 4. The $Dq$ parameter obtained (936 cm$^{-1}$) is slightly greater than in $KMgF_3:Co^{2+}$ ($Dq = 800$ cm$^{-1}$) [15]. This was expected since $Dq$ is inversely proportional to the fifth power of the distance between the ions and the ligands [24]. The lattice parameter in $BaLiF_3$ crystals (3.995 Å) is smaller than in $KMgF_3$ crystals (4.00 Å). The $B$ parameter value (875 cm$^{-1}$) in $BaLiF_3$ is close to the value in $KMgF_3:Co^{2+}$ (880 cm$^{-1}$). The reduction of the free ion $B$ parameter (972 cm$^{-1}$) in the $BaLiF_3:Co^{2+}$ is only 10%. The $C$ parameter can be obtained by a well-established relationship [23], $C \cong 4.4B$, resulting in $C = 3850$ cm$^{-1}$. The $Dq$, $B$ and $C$ parameters for the $Co^{2+}$ ions in different crystals are shown in Table 2. The spin–orbit coupling constant, $\xi$, is reduced by 10%, the same factor as for the free ion parameter $B$. For the $Co^{2+}$ free ion, $\xi$ is 550 cm$^{-1}$, thus in the $BaLiF_3:Co^{2+}$ the spin–orbit coupling constant is $\xi = 495$ cm$^{-1}$.

Besides assigning the bands to their transitions, it is necessary to know the transition character. The $^4T_1$ ($^4F$) $\rightarrow$ $^4T_2$ ($^4F$) transition has a dipole magnetic character, is spin allowed, and in the strong field approximation, involves the promotion of one electron ($t^5e^2 \rightarrow t^4e^3$). At low temperatures three pure electronic sharp lines are expected, corresponding to the $^4T_1$ ($\Gamma_6$) $\rightarrow$ $^4T_2$ ($\Gamma_6$, $\Gamma_8^a$, $\Gamma_8^b$) spin–orbit transitions, plus the vibronic components of the transition. The transition to the fourth level ($\Gamma_7$) is forbidden

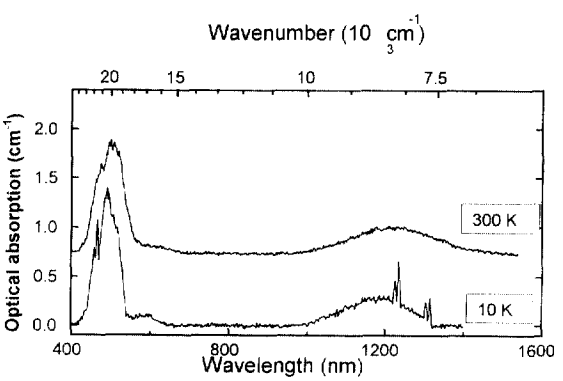


Fig. 3. Absorption spectra of the $BaLiF_3:Co^{2+}$ crystal, 0.44 mol% Co concentration, at 10 K and 300 K.

Table 1
Optical transitions, FWHM, absorption cross-section ($\sigma_A$) and oscillator strength ($f$) determined for $BaLiF_3:Co^{2+}$

| Transition | Wavenumber $cm^{-1}$ (nm) | FWHM % | Absorption cross-section $\times 10^{-20}$ $cm^2$ | Oscillator strength $\times 10^{-6}$ 11 K (291 K) |
|---|---|---|---|---|
| $^4T_1(^4F) \rightarrow {}^4T_1(^4P)$ | 20000 (500) | 17.6 | 2.0 | 1.6 (1.7) |
| $^4T_1(^4F) \rightarrow {}^4A_2(^4F)$ | 16667 (600) | 16.8 | 0.13 | 2.3 (2.4) |
| $^4T_1(^4F) \rightarrow {}^4T_2(^4F)$ | 8264 (1210) | 21.4 | 0.44 | 9.8 (9.9) |

in cubic symmetry, although it is allowed if the symmetry is reduced by stress [27]. Nevertheless, two sharp line groups are observed with these characteristics, as shown in the inset of Fig. 5, denoted by (a) and (b). It is seen that there are three peaks, corresponding to the predicted transitions among the spin–orbit splitting described before [$^4T_1(\Gamma_6) \rightarrow {}^4T_2(\Gamma_6)$; $^4T_1(\Gamma_8) \rightarrow {}^4T_2(\Gamma_8^a)$ and $^4T_1(\Gamma_6) \rightarrow {}_4T^2(\Gamma_8^b)$]. Two of them are hidden by the low intensity and spectral resolution in Fig. 5a, but are clearly seen in Fig. 5b, where they are more intense. The observed spin orbit splitting can be taken from Fig. 5a and its value is 60 $cm^{-1}$ between the two extreme peaks. The same value is obtained from Fig. 5b. This spin orbit splitting value is much smaller than the theoretically predicted one (450 $cm^{-1}$). This splitting reduction can be explained by the dynamical Jahn–Teller effect [28], and it was also observed in the $KMgF_3:Co^{2+}$ [27] and $KMgF_3:V^{2+}$ [29] systems. A comparison between the $BaLiF_3:Co^{2+}$ and the $KMgF_3:Co^{2+}$ systems shows a remarkable coincidence between the transition energy differences of the two systems, as shown in Table 3 (energy of the $^4T_1(\Gamma_6) \rightarrow {}^4T_2(\Gamma_6)$ transition and energy of $^4T_1(\Gamma_6) \rightarrow {}^4T_2(\Gamma_8^b)$ transition is 10 $cm^{-1}$ for both systems; energy of the $^4T_1(\Gamma_6) \rightarrow {}^4T_2(\Gamma_6)$ transition and energy of $^4T_1(\Gamma_6) \rightarrow {}^4T_2(\Gamma_8^a)$ transition is $\sim 60$ $cm^{-1}$ for both systems). Therefore, each group of transition lines shown in Fig. 5a, 5b match the expected behavior of the counterpart system $KMgF_3:Co^{2+}$. But only one group of lines is expected for such a system. The transition energy predicted by the energy level diagram takes into account the 8100 $cm^{-1}$ transition group (Fig. 5b). The main difference between the two groups of lines is its relative position and their spectral width (FWHM), as also shown in Table 3. All the above considerations make us conclude that these two groups of transitions are spin orbit transitions to two slightly different sites for the Co ion, and therefore we assign the group of transitions shown in Fig. 5a as the group $^4T_1(\Gamma_6^*) \rightarrow {}^4T_2(\Gamma_6^*)$; $^4T_1(\Gamma_6^*) \rightarrow {}^4T_2(\Gamma_8^{*a})$ and $^4T_1(\Gamma_6^*) \rightarrow {}^4T_2(\Gamma_8^{*b})$. Table 3 shows the transition energies for these groups of lines.

The two zero phonon sharp lines (curve a of the inset of Fig. 5) correspond to the spin–orbit transitions of the $Co^{2+}$ ion in a pure octahedral symmetry, as it is also seen in the $KMgF_3:Co^{2+}$ system [15]. Each group of lines, shown in Fig. 5, corresponds to the group of the $KMgF_3:Co^{2+}$ system. Hence the sharp line group at 7610 $cm^{-1}$ and that at 8100 $cm^{-1}$ should be replicas of the spin–orbit transitions and one of them is originated by a perturbation process, indicating two different possible sites for the $Co^{2+}$.

The origin of the two additional bands in $BaLiF_3:Co^{2+}$ at 7600 $cm^{-1}$ (presenting FWHM = 24 $cm^{-1}$ and half the intensity of the main lines at 8100 $cm^{-1}$) has not been previously established, but they were observed in $Ni^{2+}:BaLiF_3$ crystals as well [11]. In the next subsection a new hypothesis for these extra sharp lines is discussed.

These lines could be due to $Co^{2+}$ ions being in sites of other symmetry than the expected site, that presents octahedral symmetry. The $Co^{2+}$ ion could replace the $Ba^{2+}$ ion (dodecahedral symmetry site), which in first approximation is a cubic symmetry site. Additionally, the $Co^{2+}$ ion would be in a reduced local symmetry site due the

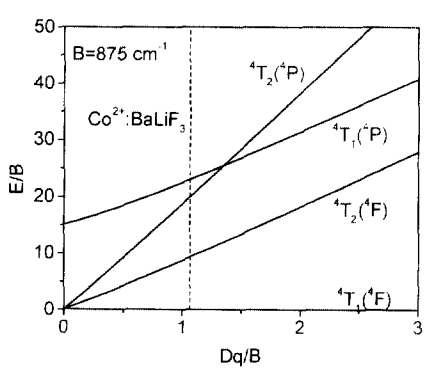


Fig. 4. $BaLiF_3:Co^{2+}$ Tanabe–Sugano energy diagram for the quartet terms. The Racah parameter $B$ is equal to 875 $cm^{-1}$.

Table 2
The crystal field parameter $Dq$, and the Racah parameters $B$ and $C$ for the $Co^{2+}$ ion, free and in a crystal

| Matrix | $Dq$ | $B$ | $C$ | $C/B$ |
|---|---|---|---|---|
| $KMgF_3$ [15] | 800 | 880 | 3872 | 4.40 |
| $KCoF_3$ [15] | 770 | 880 | 3872 | 4.40 |
| MgO [24] | 927 | 845 | 3802 | 4.5 |
| ZnO[a] [24] | 390 | 700 | 3150 | 4.5 |
| $BaLiF_3$[b] | 936 | 875 | 3850 | 4.40 |
| free ion [15] | – | 972 | 4277 | 4.40 |

[a] Tetrahedral symmetry.
[b] Data obtained in this work.

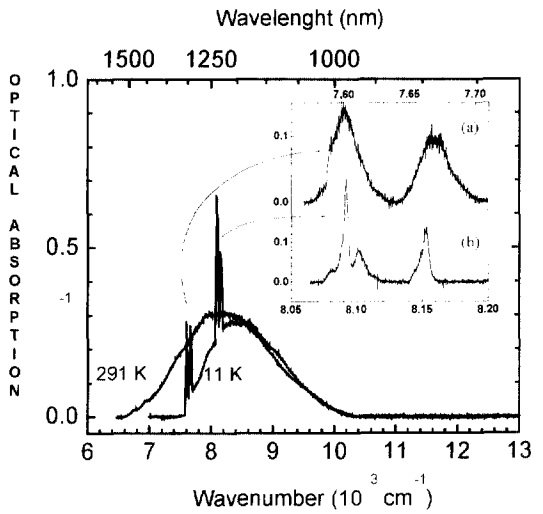


Fig. 5. Optical absorption bands in the infrared region for the $BaLiF_3:Co^{2+}$ crystal, 0.44 mol% Co concentration, at 11 K and 291 K. The two sharp line groups are magnified in the inset, denoted by (a) at 7610 $cm^{-1}$ and (b) at 8100 $cm^{-1}$.

perturbation induced by the charge compensation mechanism. There is also the hypothesis of another impurity present in the crystal arousing the extra lines [15]. As the chemical analysis of the samples used in this work showed that other dopants are in concentration smaller than 50 times the Co concentration, this hypothesis was disregarded. This same hypothesis was also discarded in the $BaLiF_3:Ni^{2+}$ work [11]. The pair effect arises as the impurity concentration increases for transition metal ions in ionic hosts, but concentrations of the order of 1 mol% are not enough to arouse these effects. Consequently, the most probable hypothesis for the extra sharp lines is that they are caused by the $Co^{2+}$ ion in a perturbed octahedral symmetry site, probably due to the charge compensation mechanism, but the site location is still unclear. A charge compensation was suggested by Leckebusch [30] consisting of a $Li^+$ associated to a vacancy, but the sharp line sets were not observed in this work, so the exact cause of these lines remains unknown.

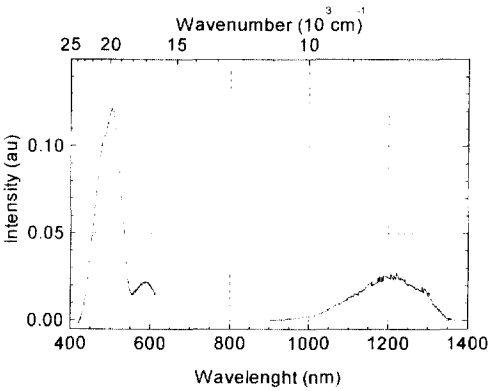


Fig. 6. Optical excitation spectra of the $BaLiF_3:Co^{2+}$ crystal, 0.44 mol% Co concentration, at 12 K.

The three absorption bands observed are electric dipole forbidden by the transition rules (the transitions are between states of the same level 3d, $\Delta L = 0$), but they are allowed by magnetic dipole and spin ($\Delta S = 0$). The oscillator strengths obtained, and shown in Table 1, ratify this consideration, since they are typical of this kind of transition of the order of $10^{-6}$.

### 3.2. Excitation spectroscopy

The excitation spectroscopy technique allows the determination of how the excited states contribute to a specific emission. In the case of simple systems, when there is only one emission channel and few energy levels, such as in $BaLiF_3:Co^{2+}$, the excitation spectrum does not add much information. The obtained excitation spectrum for the $BaLiF_3:Co^{2+}$ 0.44 mol% concentration sample is shown in Fig. 6 and reproduces the absorption band spectrum, as expected.

To obtain the excitation spectrum the broad band fluorescence peak (centered at 1500 nm) was used as the monitoring wavelength. It is often necessary to know the spectral intensity of the excitation beam. To normalize the average detected signal, with respect to variations in the spectral intensity of the excitation source, a brightness

Table 3
Energy levels and attributions to the lines for the $BaLiF_3:Co^{2+}$ crystal and for the corresponding lines in $KMgF_3:Co^{2+}$ for the $^4T_1$ ($^4F$) → $^4T_2$ ($^4F$) transition

| Transition | $BaLiF_3:Co^{2+}$ | | $KMgF_3:Co^2$ [27] | |
|---|---|---|---|---|
| | Wavenumber ($cm^{-1}$) | FWHM ($cm^{-1}$) | Wavenumber ($cm^{-1}$) | FWHM ($cm^{-1}$) |
| $\Gamma_6$ | 8092 ± 1 | 4.7 | 6914 ± 2 | 4 |
| $\Gamma_8^b$ | 8102 ± 2 | 11 | 6924 ± 2 | 7 |
| $\Gamma_8^a$ | 8153 ± 1 | 6.8 | 6984 ± 2 | 8 |
| $\Gamma_7$ | – | – | – | – |
| $\Gamma_6^*$, $\Gamma_8^{b*}$ | 7600 ± 2 | 24 | – | – |
| $\Gamma_8^{a*}$, $\Gamma_7^*$ | 7668 ± 2 | 24 | – | – |

intensity detector based on the photo-acoustic effect was used [31].

### 3.3. Emission spectrum

A conventional set up (right angle excitation and detection geometry) was used to measure the emission spectrum and the signal-to-noise ratio was maximized using the AC lock-in technique. The $BaLiF_3:Co^{2+}$ crystal presents a single emission band in the near infrared region, which is characteristic of $Co^{2+}$ ions in octahedral symmetry [12,14]. This emission band is typically composed by a vibronic broad band which is connected to the $^4T_2$ ($^4F$) $\rightarrow$ $^4T_1$ ($^4F$) transition and two pure electronic lines separated by approximately 1000 $cm^{-1}$.

Fig. 7 shows the emission spectrum at 12 K of a $BaLiF_3:Co^{2+}$ sample of 0.44 mol% Co concentration with spectral resolution of 0.4 $cm^{-1}$. It is possible to observe the spin–orbit line transitions, even with low signal-to-noise ratio, at low temperatures, since the excited state vibrational levels are not significantly thermally populated. The emission band at 12 K is centered at 6670 $cm^{-1}$ (1500 nm) with a FWHM of 1170 $cm^{-1}$ (260 nm). For the $BaLiF_3:Co^{2+}$ the spin–orbit splitting between the levels $\Gamma_6$ and $\Gamma_8$ of the ground state is 990 $cm^{-1}$, which shows good agreement with the value of 950 $cm^{-1}$ obtained for $KMgF_3:Co^{2+}$ [32].

Two pure electronic lines (no-phonon lines), one at 6603 $cm^{-1}$ attributed to the $^4T_2$ ($\Gamma_6$) $\rightarrow$ $^4T_1$ ($\Gamma_8$) transition and another at 7593 $cm^{-1}$ attributed to the $^4T_2$ ($\Gamma_6$) $\rightarrow$ $^4T_1$ ($\Gamma_6$) transition are shown. For the two pure electronic sharp lines we observed a FWHM of 20 $cm^{-1}$. The low intensity and the broad spectral width of these electronic lines are evidences that these lines were not completely isolated from the vibrational levels and are not

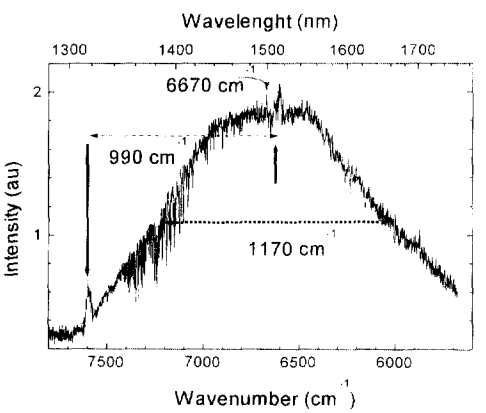


Fig. 7. Luminescent emission spectrum of $BaLiF_3:Co^{2+}$ crystal, 0.44 mol% Co concentration, at 12 K. The emission band is centered at 6670 $cm^{-1}$ (1500 nm) and presents a FWHM equal to 1170 $cm^{-1}$ (260 nm). The spin–orbit splitting between the $\Gamma_6$ and $\Gamma_8$ ground state levels is 990 $cm^{-1}$.

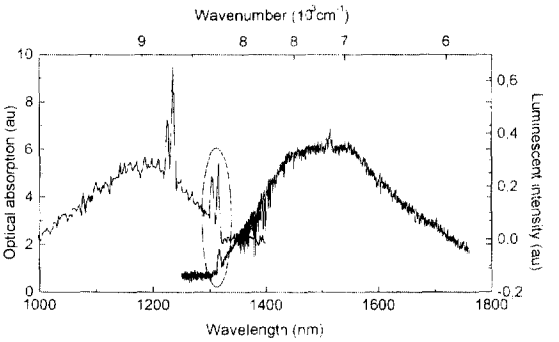


Fig. 8. $BaLiF_3:Co^{2+}$ absorption and emission spectra, at 12 K, 1 $cm^{-1}$ resolution (absorption) and 0.4 $cm^{-1}$ resolution (emission).

pure electronic lines, but otherwise are mixed with other vibrational modes existent in the crystal lattice. It is important to point out that these lines should have FWHM in the order of 5 $cm^{-1}$, as were observed in the absorption spectrum no-phonon lines and can be seen in Table 3.

The room temperature spectrum could not be observed due to a strong quenching of the luminescence. Another important effect to consider is the decrease of the luminescent intensity as a function of the pumping duration, due to local heating on the sample. The same effect was observed for $KZnF_3:Co^{2+}$ crystals [33].

By overlapping the absorption and emission spectra it is possible to observe that the pure electronic line $^4T_1$ ($G_6$) $\leftrightarrow$ $^4T_2$ ($G_6$) of the absorption spectrum coincides in energy with the sharp line in the emission spectrum (Fig. 8), indicating that they have the same origin, as expected. This fact leads to the conclusion that the emission band is a magnetic dipole allowed transition.

The energy level diagram with the spin–orbit splitting for a $Co^{2+}$ ion in $KMgF_3$ [32] is shown in Fig. 9. These values are very similar to the values found for $KZnF_3:Co^{2+}$

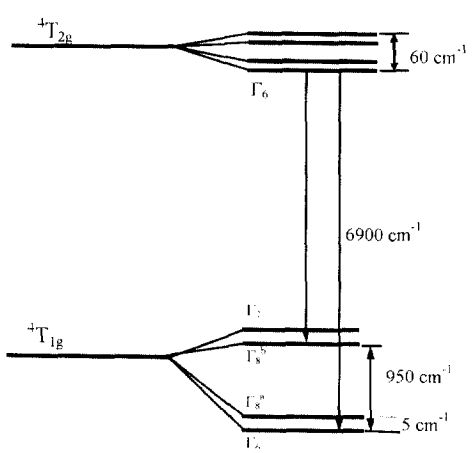


Fig. 9. Energy levels diagram with the spin–orbit splitting for the $^4T_2 \rightarrow {}^4T_1$ transition of the ion $Co^{2+}$ in $KMgF_3$ [32].

[33] and it is expected that they are close to the values for $BaLiF_3:Co^{2+}$, since the only influential factor in the spin–orbit splitting is the spin–orbit coupling constant, $\zeta$, which induces a very small variation in the position of the energy levels (of only few $cm^{-1}$) in the case of $Co^{2+}$ in octahedral symmetry.

The phonon energy for the $BaLiF_3$ crystal is $h\omega = 509$ $cm^{-1}$ [34] and the Huang–Rhys factor ($S_0$) (given by Stokes' shift $= 2S_0 h\omega = E_{ABS} - E_{EM} = 2036$ $cm^{-1}$) is $S_0 = 4$, which represents the average number of phonons involved in the optical transition. The value found for $BaLiF_3:Co^{2+}$ perfectly agrees with the values obtained for the $Co^{2+}$ ion in other ionic crystals ($S = 4$ to 5 [33]).

## 4. Conclusion

In this work, the spectroscopic properties of $BaLiF_3:Co^{2+}$ crystals were studied. Three absorption bands were identified in the $BaLiF_3:Co^{2+}$ crystal. The main absorption band peaks at 20 000 $cm^{-1}$ (500 nm) and 8264 $cm^{-1}$ (1210 nm), correspond to the $^4T_1\ (^4F) \rightarrow {}^4T_1(^4P)$ and $^4T_1(^4F) \rightarrow {}^4T_2(^4F)$ transitions, respectively. These bands were identified by the direct absorption spectrum as well as by the excitation spectrum. Besides these two bands there is a weaker band at 16 667 $cm^{-1}$ (600 nm), which corresponds to the $^4T_1\ (^4F) \rightarrow {}^4A_2\ (^4F)$ transition. The optical absorption spectra obtained for $BaLiF_3:Co^{2+}$ are similar to the spectra reported for $Co^{2+}$ in other ionic hosts of the fluoroperovskite family, for example the $KMgF_3:Co^{2+}$, and the $MgO:Co^{2+}$, where the $Co^{2+}$ occupy a site of octahedral symmetry. Based on the absorption spectra we can affirm that there are two dominant $Co^{2+}$ sites. However, further work is required to establish the process responsible for the charge compensation.

The crystal field parameter ($Dq$) and the Racah parameters ($B$ and $C$) were determined using the Tanabe–Sugano energy levels diagram. The resulting fitting parameters for the $BaLiF_3:Co^{2+}$ crystal are $Dq = 936$ $cm^{-1}$ and $B = 875$ $cm^{-1}$.

The $BaLiF_3:Co^{2+}$ crystal presents an emission in the region of 1500 nm (6670 $cm^{-1}$), attributed to the $^4T_2\ (^4F) \rightarrow {}^4T_1\ (^4F)$ transition, with FWHM of 260 nm, at 12 K. This single broad band emission observed is characteristic of a $Co^{2+}$ ion in a octahedral site and it is observed by pumping in any of the absorption bands. The particular interest to study $BaLiF_3:Co^{2+}$ came from its possible laser emission region, around 1500 nm, which lies on the low loss window for telecommunication fiber transition. However, the strong luminescence thermal quenching, going from 10 to 300 K, indicates that this laser should be operated at low temperature. The results obtained up to now show the $BaLiF_3:Co^{2+}$ crystal as a promising material for laser operation, either pumped by a flash lamp or a Nd:YAG laser.

## Acknowledgements

M. Duarte and E. Martins wish to thank CNPq/RHAE and FAPESP for their scholarships. This work was partially supported by FAPESP.

## References

[1] P.F. Moulton, Solid State Research Rep. DTIC AD-A124305/4 (1982:3), M.I.T. Lincoln Lab., Lexington, 1982, pp. 15.
[2] J.C. Walling, in: L.F. Mollenauer, J.C. White (Eds.), Tunable Paramagnetic-ions Solid-state Lasers, Tunable Lasers Topics in Applied Physics, vol. 59, ch. 9, Springer Series, 1987, p. 331.
[3] L.F. Mollenauer, J.C. White (Eds.), Tunable Lasers Topics in Applied Physics, vol. 59, Springer Series, 1987.
[4] A. Penzkoffer, in: Solid State Lasers, Prog. Quant. Electron., vol. 12, Pergamon, Oxford, 1988.
[5] W. Gellermann, C.R. Pollock, F. Luty, Optics Comm. 39 (1981) 391.
[6] P.F. Moulton, IEEE J. Quantum Electron. QE 18 (1982) 1185.
[7] A. Sennaroglu, C.R. Pollock, Optics Lett. 19 (1994) 390.
[8] M. Duarte, M.M.F. Vieira, S.L. Baldochi, Mater. Sci. Eng. B 25 (1994) 133.
[9] L. Prado, N.D. Vieira Jr., S.L. Baldochi, S.P. Morato, J.Y. Gesland, Solid State Commun. 87 (1993) 41.
[10] L. Prado, N.D. Vieira Jr., S.L. Baldochi, S.P. Morato, J.P. Dennis, N. Tercier, B. Blanzat, J. Phys. Chem. Solids 57 (1996) 413.
[11] E. Martins, N.D. Vieira Jr., S.L. Baldochi, S.P. Morato, J.Y. Gesland, J. Luminesc. 62 (1994) 281.
[12] E. Martins, M. Duarte, S.L. Baldochi, S.P. Morato, M.M.F. Vieira, N.D. Vieira Jr., J. Phys. Chem. Solids 58 (1997) 655.
[13] N.L. Rowell, D.J. Lockwood, J. Electrochem. Soc. 136 (1989) 3536.
[14] S.L. Baldochi, J.Y. Gesland, Mater. Res. Bull. 27 (1992) 891.
[15] J. Fergusson, D.L. Wood, K. Knox, J. Chem. Phys. 39 (1963) 881.
[16] W. Low, Phys. Rev. 109 (1958) 1256.
[17] W.L. Powell, D.J. Lockwood, J. Luminesc. 40/41 (1988) 629.
[18] U. Dürr, Laser Optoelectron. 15 (1983) 31.
[19] P. Hammerling, A.B. Budgor, A. Pinto (Eds.), Tunable Solid-state Lasers, Optical Sciences, vol. 47, Springer Series, 1985.
[20] L.F. Johnson, H.J. Guggenheim, R.A. Thomas, Phys. Rev. 149 (1966) 197.
[21] S.L. Baldochi, A.M.E. Santo, E. Martins, M. Duarte, M.M.F. Vieira, N.D. Vieira Jr., S.P. Morato, J. Cryst. Growth 166 (1996) 375.
[22] A.V. Chadwick, S.R. Davis, J.F. de Lima, M.E.G. Valerio, S.L. Baldochi, J. Phys. Condens. Matter 8 (1996) 10679.
[23] A. Mooradian, Rep. Prog. Phys. 42 (1979) .
[24] R. Pappalardo, D.L. Wood, R.C. Linares Jr., J. Chem. Phys. 35 (1961) 2041.

[25] R.G. Buns, Mineral Applications of Crystal Field Theory, Cambridge University Press, London, 1970.
[26] S. Sugano, Y. Tanabe, H. Kamimura, in: Multiplets of Transition Metal Ions in Crystals, Academic Press, New York, 1970.
[27] M.D. Sturge, H.J. Guggenheim, Phys. Rev. B 4 (1971) 2092.
[28] F.S. Ham, Phys. Rev. 138 (1965) A1727.
[29] M.D. Sturge, Phys. Rev. B 1 (1970) 1005.
[30] R. Leckebusch, A. Neuhaus, K. Recker, J. Cryst. Growth 16 (1972) 10.
[31] M. Duarte, I.M. Ranieri, M.M.F. Vieira, Opt. Mater. 3 (1994) 269.
[32] M.D. Sturge, Phys. Rev. B 8 (1973) 6.
[33] W. Künzel, W. Knierim, U. Dürr, Optics Comm. 36 (1981) 383.
[34] A. Boumriche, P. Simon, M. Rousseau, J.Y. Gesland, F. Gervais, J. Phys. Condens. Matter 1 (1989) 5613.